APPLYING VECTOR BOSON FUSION TOPOLOGIES TO SEARCH FOR SUPERSYMMETRIC AND HIGGS PORTAL DARK MATTER AT THE LHC

A Dissertation

by

SEAN DANIEL WU

Submitted to the Office of Graduate and Professional Studies of
Texas A&M University
in partial fulfillment of the requirements for the degree of

DOCTOR OF PHILOSOPHY

Chair of Committee,	Bhaskar Dutta
Committee Members,	Teruki Kamon
	Louis Strigari
	Stephen Fulling
Head of Department,	Peter McIntyre

August 2017

Major Subject: Physics

ABSTRACT

This work presents two searches for dark matter at the Large Hadron Collider (LHC). The first is focused on decays of the supersymmetric partner of the top quark, the stop quark ($\tilde{t}$). By exploiting vector boson fusion (VBF) topologies, the analysis shows a top squark with mass of 300 GeV and integrated luminosity of 300 fb^{-1} can be probed at 5σ significance with no systematic uncertainty. The second search is a study of Higgs portal dark matter (HPDM). In order to study HPDM, we consider two boosted channels. The first is a study of vector boson fusion production. Here we show the differences between the $\not{E}_{\mathrm{T}}$ distribution for HPDM and wino dark matter. We also show the significance as a function of DM mass. The second channel for HPDM is $Z + H$ production of DM. In this case, we are interested in trying to differentate between fermionic, scalar, and vector DM. We show kinematic distributions for these three cases. Additionally, we consider the influence of the Higgs width on these kinematic distributions for the fermionic case.

DEDICATION

This work is dedicated to my friends and family whose continued love and support has made my academic career possible.

ACKNOWLEDGMENTS

I am grateful to my advisor Bhaskar Dutta for his guidence, feedback, and encouragement. He has had a profound influence on my work, but he has also had a great deal of influence on me as a person and developing professional. His kindness, patience, and optimism will be missed as I am moving forward in my career.

I also owe a great deal of thanks to Teruki Kamon. Teruki's unparalleled eye for detail has motivated me to put forward the best work I possibly can. It has been a great pleasure working with a scientist of Teruki's caliber.

I would also like to offer special thanks to Tathagata Ghosh and Kuver Sinha whose discussions and mentoring have been instrumental in my development as a student.

I would like to thank my collaborators Will Flanagan, Kenichi Hatakeyama, Alfredo Gurrola, Will Johns, Paul Sheldon, and Zhenbin Wu.

I would like to acknowledge Mykhailo Dalchenko, Yu Gao, Peisi Huang, Nikolay Kolev, Denis Rathjens, and Joel Walker for their insight over the years. Our weekly meetings have been a tremendous influence on me.

Finally I would like to thank my friends and office-mates Stephen Clark, Esteban Jimenez, Junchen Rong, and Benjamin Schroeder.

CONTRIBUTORS AND FUNDING SOURCES

Contributors

This work was supported by a dissertation committee consisting of Professors Bhaskar Dutta, Teruki Kamon, and Louis Strigari the Department of Physics and Professor Stephen Fulling of the Department of Mathematics.

Chapter 3 contains a reprint of an article entitled "Probing Compressed Top Squarks at the LHC at 14 TeV." This work was completed in association with Bhaskar Dutta, Will Flanagan, Alfredo Gurrola, Will Johns, Teruki Kamon, Paul Sheldon, Kuver Sinha, and Kechen Wang and is reprinted with permission from the American Physical Society.

All other work conducted for the dissertation was completed by the student independently.

Funding Sources

This work was made possible in part by the Department of Energy under Grant Number DE-FG02-13ER42020.

Its contents are solely the responsibility of the authors and do not necessarily represent the official views of the Department of Energy.

NOMENCLATURE

DM	Dark Matter
CDM	Cold Dark Matter
SM	Standard Model
HPDM	Higgs Portal Dark Matter
HPS	Higgs Portal Scalar
HPF	Higgs Portal Fermion
HPV	Higgs Portal Vector
BSM	Beyond the Standard Model
LSP	Lightest Supersymmetric Particle
VBF	Vector Boson Fusion
LHC	Large Hadron Collider
CMS	Compact Muon Solenoid
ATLAS	A Toroidal LHC ApparatuS
CL	Confidence Level
QCD	Quantum Chromodynamics
QED	Quantum Electrodynamics
t	Top Quark
$\tilde{t}$	Top Squark
$\tilde{\chi}_1^0$	Neutralino One
$\not{E}_{\mathrm{T}}$	Missing Transverse Energy
eV	Electronvolts

fb	Femptobarn
$\tilde{q}$	Squark
$\tilde{g}$	Gluino
m_X	Mass of X
$\tilde{\chi}_1^{\pm}$	Chargino
m_T	Transverse Mass
b	Bottom Quark
W	W Boson
Z	Z Boson
V	Inclusive W and Z Bosons
l	Lepton
p_T	Transverse Momentum
η	Pseudorapidity
H	Higgs Boson
VEV	Vacuum Expectation Value
ILC	International Linear Collider
VDM	Vector Dark Matter

TABLE OF CONTENTS

Page

LIST OF FIGURES

FIGURE Page

LIST OF TABLES

1. INTRODUCTION

The Standard Model (SM) is the most complete picture of known particle phenomena. It accurately provides a unifying picture of the strong and electroweak forces. Through the Higgs mechanism, it explains why particles have mass. Since its inception, experimental physics has pushed the energy threshold into the TeV range and still the Standard Model is the basis of understanding for the interactions of baryons, leptons, and gauge bosons.

As successful a theory as it is, the Standard Model does not address many underlying problems in particle physics. It does not provide any prediction for neutrino mass. Nor does it address the hierachy problem. (The large difference between the electroweak scale and the Planck scale and why the Standard Model Higgs boson has a relatively small mass). Perhaps most conspicuously, it does not address problems of observational cosmology. That is, it does not address baryon asymmetry nor does it provide a candidate for dark matter. Additional theories are required in order to address these problems.

Supersymmetry is a leading candidate for physics beyond the standard mode as it addresses several of these problems. Supersymmetry doubles the number of standard model particles such that each fermion has an associated boson, and each boson has an associated fermions. By adding these additional particles, the quadratic divergences to the Higgs mass loop can be canceled which stablizes the Higgs mass to its observed value. Because third generation quarks couple most strongly the the Higgs, finding the superpartner for the top quark is imperative in order to address this issue.

Supersymmetry can also provide an explanation for the dark matter content in the universe. The lightest supersymmetric particle (LSP) can provide a suitable dark matter candidate. The small annihilation cross section of pure bino LSP of mass of around 100 GeV makes it difficult to reproduce the observed dark matter relic density [2]. However, in

the case where the lightest $\tilde{t}$ is close to the $\tilde{\chi}_1^0$ mass, co-annihilation of $\tilde{t}$ pairs can produce the proper relic density [3].

Another leading theory to provide a stable dark matter candidate is to extend the standard model Higgs. These models are very well motivated because they are an extension of an observed particle. If additional Higgses are observed that mix with the standard model Higgs, these Higgses can couple to dark matter. Observation of the decay of these additional Higgses can provide an explanation of the dark matter content of the universe.

This work will present two studies of theories beyond the standard model (BSM) and their experimental implications at the Large Hadron Collider. The next chapter is a general overview of VBF. We describe the kinematic signatures of VBF and consider the implications of studying these types of scenarios. The following chapter is a study of compressed top squarks ($\tilde{t}$) decays [1]. This is a scenario where the stop mass is degenerate with the sum of the top mass and the lightest neutralino ($\tilde{\chi}_1^0$). We consider the implications of studying this scenario by using VBF. The final chapter is a study of Higgs portal dark matter (HPDM). We consider two scenarios for boosting these systems. The first is to apply VBF. The second is to consider $Z + H$ production where the Z boson boosts the Higgs boson.

2. VECTOR BOSON FUSION

Vector Boson Fusion (VBF) is a category of processes in which incident quarks scatter via t-channel exchange of vector bosons, typically W or Z bosons or photons. Through the interaction of these vector bosons, secondary particles can be produced. Figure 2.1 shows an example of a VBF process. Here up quarks radiate Z bosons which in turn interact to create a Higgs Boson.

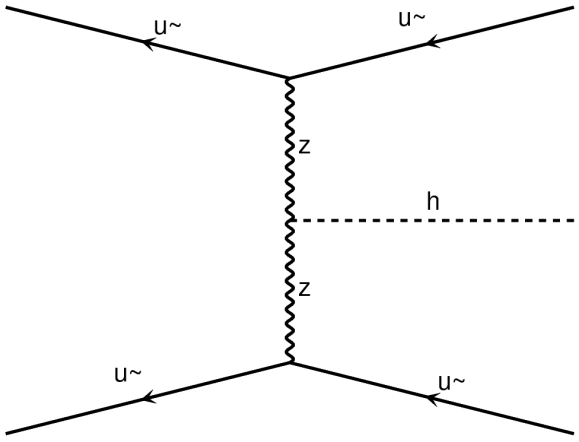

Figure 2.1: Sample VBF Feynman Diagram for Higgs production via ZZ fusion. Produced using Madgraph5

Vector Boson Fusion processes provide favorable kinematic signatures in order to study new physics at collider experiment. VBF processes are characterized by two jets with large invariant mass in opposite hemispheres and large separation in pseudorapidity (η). Figure 2.2 shows what a typical VBF event looks like at a collider experiment.

In order to study these types of events, the following cuts are applied to the two jets in an event with the largest invariant mass:

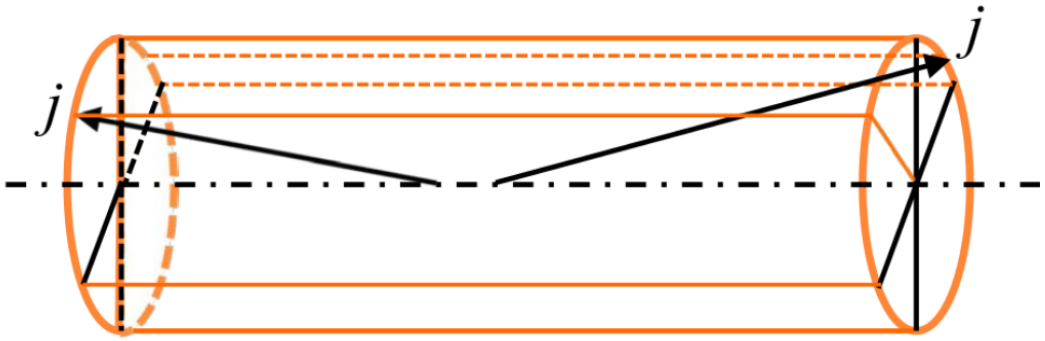

Figure 2.2: Illustration of a VBF signature at collider experiment. Credit: Kechen Wang

- $p_T > 50.$
- $|\Delta\eta(j_1, j_2)| > 3.5$
- $\eta_1 \cdot \eta_2 < 0$
- $m_{j_1 j_2} > 500$ GeV

The virtue of studying systems of this type is the fact that VBF jets boost the rest of the system in the transverse plane. In systems with large $\not{E}_{\mathrm{T}}$, this $\not{E}_{\mathrm{T}}$ is enhanced in order to balance the momentum of the jets. This makes VBF an effective strategy to search for Dark Matter.

VBF is also useful in studying compressed scenarios in which leptons have small transverse momentum. In [4] we showed that even when the differences between $m_{\tilde{\mu}}$ and $m_{\tilde{\chi}_1^0}$ is small, the boosting of the slepton system allows for detection of soft leptons. Figure 2.3 shows this explicitly.

This work will present two additional applications of VBF. The first is a study of compressed stop quarks. This is a scenario where the mass of the stop quark is nearly degenerate with the mass of the lightest neutralino and the mass of the top. We show that vector boson fusion is effective in boosting the stop system and enhancing the $\not{E}_{\mathrm{T}}$. The

second is a study of Higgs portal dark matter. This is a scenario where the Higg's boson couples to dark matter. We show that applying Vector Boson Fusion topologies to this scenario is effective in boosting the $\not{E}_{\mathrm{T}}$ and ultimately allows us to distinguish between HPDM and Wino DM.

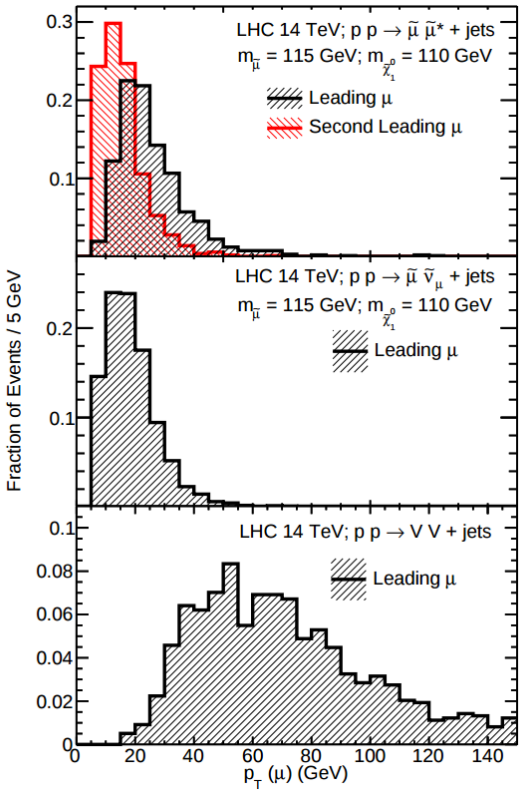

Figure 2.3: Plot of muon p_T for compressed smuon scenario after VBF cuts. Plots show that despite the small mass gap between smuon and $\tilde{\chi}_1^0$ is small, selection of the boosted system allows detection of soft leptons.

3. SEARCHING FOR COMPRESSED STOP QUARKS*

3.1 Overview

Weak-scale supersymmetry is a leading candidate for physics beyond the Standard Model (SM), as it addresses the hierarchy problem, gives gauge coupling unification, and (in R-parity conserving models) provides a robust dark matter (DM) candidate.

The search for colored superpartners at the Large Hadron Collider (LHC) has so far yielded null results. The exclusion limits on squark ($\tilde{q}$) and gluino ($\tilde{g}$) masses, when they are comparable, are approximately 1.5 TeV at 95% CL with 20 fb^{-1} of integrated luminosity [5, 6, 7, 8].

On the other hand, the bounds on the mass of the lightest top squark ($\tilde{t}$) are less stringent. The vanilla scenario for $\tilde{t}$ studies is to consider the direct QCD production of $\tilde{t}$ pairs which decay to the top (t) and the lightest neutralino ($\tilde{\chi}_1^0$) with 100% branching ratio. Exclusion limits in the $m_{\tilde{t}}$-$m_{\tilde{\chi}_1^0}$ plane have been obtained in this decay mode [9, 10].

The challenge of investigating $\tilde{t}$ pair production lies in the huge background from top quark pair production. For this decay topology, the particles in the final state are identical to the $t\bar{t}$ background supplemented with missing transverse energy ($\not{E}_{\rm T}$). A number of analysis strategies have been proposed recently, covering both the fully hadronic [11] as well as the semi-leptonic [12] final states. Search strategies in these final states using top taggers have also been pursued (for a review, see [13]). The projected top squark discovery mass reach and exclusion plots for the high-luminosity LHC have been studied by the ATLAS [14] and CMS [15] Collaborations. We note as an aside that a couple of studies have focussed on other decay topologies, such as $\tilde{t} \to b\tilde{\chi}_1^{\pm}$ [16], which are interesting from

*This chapter is reprinted with permission from "Probing Compressed Top Squarks at the LHC at 14 TeV" by Bhaskar Dutta, Will Flanagan, Alfredo Gurrola, Will Johns, Teruki Kamon, Paul Sheldon, Kuver Sinha, Kechen Wang, Sean Wu Phys. Rev. D 90, 095022, Copyright 2014 by The American Physical Society

the point of view of well-tempered Bino/Higgsino or pure Higgsino dark matter.

The challenge is exacerbated when the mass gap between $\tilde{t}$ and $t + \tilde{\chi}_1^0$ is small. The $m_{\tilde{t}} = m_t + m_{\tilde{\chi}_1^0}$ line on the $m_{\tilde{t}}$-$m_{\tilde{\chi}_1^0}$ plane is a virtual Rubicon, and current exclusion bounds are non-existent near it. For $m_{\tilde{t}} \sim 190 - 300$ GeV, the exclusion bounds come within $\Delta M = m_{\tilde{t}} - (m_t + m_{\tilde{\chi}_1^0}) \sim 15$ GeV. For $m_{\tilde{t}} \sim 300 - 450$ GeV, there is significant degradation and exclusions only reach $\Delta M \sim 25$ GeV. For $m_{\tilde{t}} > 450$ GeV, the smaller production cross-section leads to exclusion bounds with $\Delta M \gg 50$ GeV. The discovery reach at the 14 TeV LHC (LHC14) with 300 fb^{-1} data, assuming an optimistic projection * of LHC8 results, is similar. In this compressed scenario, search strategies that rely on $\not{E}_{\rm T}$ to reduce $t\bar{t}$ background have poor performance. The challenge is even greater when $m_{\tilde{\chi}_1^0}$ becomes vanishingly small in the compressed region, so that $m_{\tilde{t}} \sim m_t$. In this scenario, which is called the stealthy scenario ($\Delta M \sim 0$ GeV), the $\not{E}_{\rm T}$ discrimination between signal and background becomes very ineffective. These scenarios have been studied by several groups and the proposed strategies include a shape-based analysis of the $\not{E}_{\rm T}$ and m_T distributions [17], rapidity gap and spin correlation observables [18], and optimized use of dileptonic m_{T2} [19].

Similarly, probing the top squark in its three-body decay mode $\tilde{t} \to bW\tilde{\chi}_1^0$ is also difficult. The current exclusion limit on this mode at the 8 TeV LHC (LHC8) with 20 fb^{-1} of data from CMS starts from $m_{\tilde{t}} = 200$ GeV, with $\Delta M = -25$ GeV. The discovery reach at the 14 TeV LHC (LHC14) with 300 fb^{-1} data is similar. For smaller ΔM there are no limits, e.g., the limit ceases to exist for $-150 \leq \Delta M \leq -70$ GeV at $m_{\tilde{t}} = 200$ GeV. Although the current monojet searches can place contraints for $\Delta M < -150$GeV, those contraints are limited beyond $m_{\tilde{t}} = 200$ GeV.

The purpose of the current work is to propose search strategies for $\tilde{t}$ pairs in the com-

*The optimistic projection scales up N_S and $N_{\rm BG}$ by "cross-section ratio times luminosity" ratio from 8-TeV analyses with its uncertainty reduced by $1/\sqrt{r_{\rm BG}}$ or a minimum value of 10%.

pressed scenario in the small ΔM region using Vector Boson Fusion (VBF) tagging. VBF jet topologies have recently been proposed by the authors as a probe of the non-colored sector of supersymmetric models. Charged and neutral Wino production followed by decays to $\tilde{\chi}_1^0$ via a light slepton has been studied in [20, 21], while VBF searches for Wino and Higgsino DM has been proposed in [22]. The classic mechanism for VBF searches in the case of noncolored particles occurs through the fusion of the W and Z weak bosons. As shown in [20] and [22], the requirement of two energetic jets in the forward region with large dijet invariant mass is very effective in reducing SM backgrounds in the VBF analysis. The stops are produced through gluon fusion, one of the dominant sources of production in the case of colored particles. However we still require two jets in the final state with large separation in pseudorapidity and large dijet invariant mass just like the VBF searches for pure electroweak production. We refer to this type of final state as VBF topology.

In contrast to other $\tilde{t}$ searches where compressed spectra results in low $\not{E}_{\mathrm{T}}$, making it difficult to discriminate against $t\bar{t}$ background, VBF topologies naturally give rise to larger $\not{E}_{\mathrm{T}}$ since the momentum of the particles produced in the $\tilde{t}$ system must balance the high p_T of the scattered partons. Thus, in the compressed scenario, the $\tilde{\chi}_1^0$ resulting from the $\tilde{t}$ decay carries significant $\not{E}_{\mathrm{T}}$, providing better control of the $t\bar{t}$ background.

3.2 Search Strategy

For this feasibility study, inclusive $\tilde{t}\tilde{t}^* +$ multi jets samples are generated with $\tilde{t}$ masses in the range of 200-600 GeV, keeping $\Delta M \sim \pm 7$ GeV. This region is not constrained by the present limit. There also exists no limit from the projections from the 14 TeV LHC. Both QCD and weak production processes of $\tilde{t}\tilde{t}^* +$ multi-jets are included. The $\tilde{\chi}_1^0$ in our studies is mostly Bino, while the $\tilde{t}$ is mostly $\tilde{t}_R$ such that the dominant decay mode of the $\tilde{t}$ is $\tilde{t} \rightarrow t\tilde{\chi}_1^0$ in the 2 body case and $\tilde{t} \rightarrow t^*\tilde{\chi}_1^0$ in the 3 body case. The signal in both

$\Delta M \sim \pm 7$ GeV cases is 2 high p_T jets + $2b + 1l + \not{E}_{\rm T}$. The other colored particles, neutralinos and charginos are assumed to be much heavier.

Signal and background samples are generated with MADGRAPH5 [23] followed by the parton showering and hadronization with PYTHIA [24] and the detector simulation using PGS4 [25].

We use pre-cut samples for signal and background to develop our search strategies. The pre-cut sample is is obtained using MADGRAPH5run card level cuts. The search strategy is based on three steps. First, we use the unique features of VBF jet topology to reduce $V +$ jets backgrounds (where V is either W or Z). Second, we the use decay properties of the centrally produced $\tilde{t}$ pair, namely the requirement of an isolated lepton and two b-tagged jets from a top quark, to further reduce light quark QCD backgrounds and other channels that are also produced by VBF topologies. Finally, the $\not{E}_{\rm T}$ distribution is used to assess the presence of a signal above the $t\bar{t}$.

(1) VBF cuts: the event is required to have a presence of at least two jets (j_1, j_2) satisfying: (i) $p_{\rm T} \geq 75$ and 50 GeV in $|\eta| \leq 4$; (ii) $|\Delta\eta(j_1, j_2)| > 3.5$; (iii) $\eta_{j_1} \cdot \eta_{j_2} < 0$; (iv) dijet invariant mass $M_{j_1 j_2} > 500$ GeV.

(2) One isolated lepton with $p_{\rm T} \geq 20$ GeV and two loose b-jets with $p_{\rm T} \geq 30$ GeV in $|\eta| < 2.5$ are required. The b-jet identification efficiency and fake rate are taken to be 70% and 1%, respectively.

(3) In order to highlight the effectiveness of the $\not{E}_{\rm T}$ distribution after the VBF topological selections, the cut flow tables with corresponding cross-sections at each stage are displayed under different considerations of the $\not{E}_{\rm T}$ phase space (e.g. $\not{E}_{\rm T} > 100$ GeV for $m_{\tilde{t}} = 300$ GeV).

3.3 Compressed Scenario

The cut flow table with corresponding cross-sections at each stage are shown in Table 3.1 and 3.2 for $\Delta M = \pm 7$ GeV. As mentioned, the $\not{E}_{\rm T}$ cuts are very effective in improving the signal to background ratio.

Table 3.1: Compressed scenario with $\Delta M = 7$ GeV: Summary of the effective cross-sections (fb) for different benchmark signal points as well as the $t\bar{t}$ background at 14 TeV LHC. Masses and momenta are in GeV. Reprinted with permission from [1]

$(m_{\tilde{t}}, m_{\tilde{\chi}_1^0})$	Selection	Signal	$t\bar{t}$+jets	S/B
$(200, 20)$	Pre cut	5.4×10^4	6.9×10^5	—
$\Delta M = 7$	VBF	1.8×10^3	3.8×10^4	—
	1 lepton	390	8.1×10^3	—
	2 b-jets	170	3.1×10^3	5.6×10^{-2}
	$\not{E}_{\rm T} > 100$	44	680	6.5×10^{-2}
$(300, 120)$	Pre cut	7.4×10^3	6.9×10^5	—
$\Delta M = 7$	VBF	250	3.8×10^4	—
	1 lepton	56	8.1×10^3	—
	2 b-jets	32	3.1×10^3	1.0×10^{-2}
	$\not{E}_{\rm T} > 100$	8.9	680	1.3×10^{-2}
$(400, 220)$	Pre cut	1.6×10^3	6.9×10^5	—
$\Delta M = 7$	VBF	62	3.8×10^4	—
	1 lepton	14	8.1×10^3	—
	2 b-jets	8.4	3.1×10^3	2.7×10^{-3}
	$\not{E}_{\rm T} > 100$	4.8	680	7.0×10^{-3}
$(500, 320)$	Pre cut	460	6.9×10^5	—
$\Delta M = 7$	VBF	19	3.8×10^4	—
	1 lepton	4.2	8.1×10^3	—
	2 b-jets	2.4	3.1×10^3	7.9×10^{-4}
	$\not{E}_{\rm T} > 150$	1.5	250	6.0×10^{-3}

Table 3.2: Compressed scenario with $\Delta M = -7$ GeV: Summary of the effective cross-sections (fb) for different benchmark signal points as well as the $t\bar{t}$ background at LHC14. Masses and momenta are in GeV. Reprinted with permission from [1]

$(m_{\tilde{t}}, m_{\tilde{\chi}_1^0})$	Selection	Signal	$t\bar{t}$+jets	S/B
$(200, 35)$	Pre cut	5.4×10^4	6.9×10^5	—
$\Delta M = -7$	VBF	1.4×10^4	3.8×10^4	—
	1 lepton	270	8.1×10^3	—
	2 b-jets	79	3.1×10^3	2.5×10^{-2}
	$\not{E}_{\rm T} > 100$	29	680	4.3×10^{-2}
$(300, 135)$	Pre cut	7.4×10^3	6.9×10^5	—
$\Delta M = -7$	VBF	220	3.8×10^4	—
	1 lepton	43	8.1×10^3	—
	2 b-jets	12	3.1×10^3	3.7×10^{-3}
	$\not{E}_{\rm T} > 100$	6.7	680	9.8×10^{-3}
$(400, 235)$	Pre cut	1.6×10^3	6.9×10^5	—
$\Delta M = -7$	VBF	51	3.8×10^4	—
	1 lepton	10.	8.1×10^3	—
	2 b-jets	2.8	3.1×10^3	8.9×10^{-4}
	$\not{E}_{\rm T} > 200$	0.7	100	6.6×10^{-3}

After all the cuts, the $t\bar{t}$ contribution is found to be the dominant background. The $W+$ jets as well as WZ, WW events are expected to be negligible. The combined contribution from $W+$ jets, WZ, and WW events is negligible. The requirement of the presence of the isolated lepton in the signal reduces the light flavor and gluon jets from QCD processes effectively.

As ΔM increases, the b jet becomes more energetic and the signal rate improves. In order to show this feature explicitly, let us choose $m_{\tilde{t}}$=300 GeV with $m_{\tilde{\chi}_1^0} = 150$ and 135 GeV. We find that after the $\not{E}_{\rm T}$ cut, the signal cross-sections are 5.0 fb and 6.7 fb

for $m_{\tilde{\chi}_1^0} = 135$ and 150 GeV, respectively. We note that the ability to identify soft b-jets ($p_T \sim 20$GeV) in a high pileup environment of the LHC14 is an important requirement for this analysis.

Figure 3.1 shows the distributions of $\not{E}_{\rm T}$ normalized to unity for signal (green horizontally dashed histogram) and $t\bar{t}$+jets background (red diagonally dashed histogram) after VBF selections and lepton and b-jet requirements for two benchmark points $\Delta M = 7$ GeV and $\Delta M = -7$ GeV. From the figure, it is clear that the signal shows up as a broad enhancement in the tail of the $\not{E}_{\rm T}$ distribution.

It is clear from Figure 1 that there is significant benefit from prusuing a shape based analysis using the $\not{E}_{\rm T}$ distribution and the shape of the $\not{E}_{\rm T}$ distribution shows difference between $\Delta M = 7$ and $\Delta M = -7$ GeV. We indeed propose such a strategy and those results will be presented.

We can calculate the significances $S/\sqrt{S+B}$, where S and B are the signal and background yields respectively, using a simple cut and count approach with the $\not{E}_{\rm T}$ preselections used in Tables I and II, keeping $\Delta M = \pm 7$ GeV, for various values of integrated luminosity at LHC14. We find that for ΔM =7 GeV $m_{\tilde{t}} \sim 390$ GeV (320 GeV) can be probed at 3σ (5σ) level with 300 fb^{-1} of integrated luminosity. The reach increases to 560 GeV (470 GeV) at 3σ (5σ) for 3000 fb^{-1} of luminosity. For the three body case with $\Delta M = -7$ GeV, the reach for $\tilde{t}$ is 320 (275) GeV at 3σ (5σ) with 300 fb^{-1} and 440 (380) GeV at 3σ (5σ) with 3000 fb^{-1} integrated luminosity.

3.4 Systematics

The signal sensitivity considered thus far does not consider any source of systematic uncertainty. In Fig.3.2 we show signal significances under the consideration of of 3, 5 or 10% for $\Delta M = \pm 7$ GeV. The shape based analysis of the $\not{E}_{\rm T}$ distribution is performed using a binned likelihood following the test statistic based on the profile likelihood ratio.

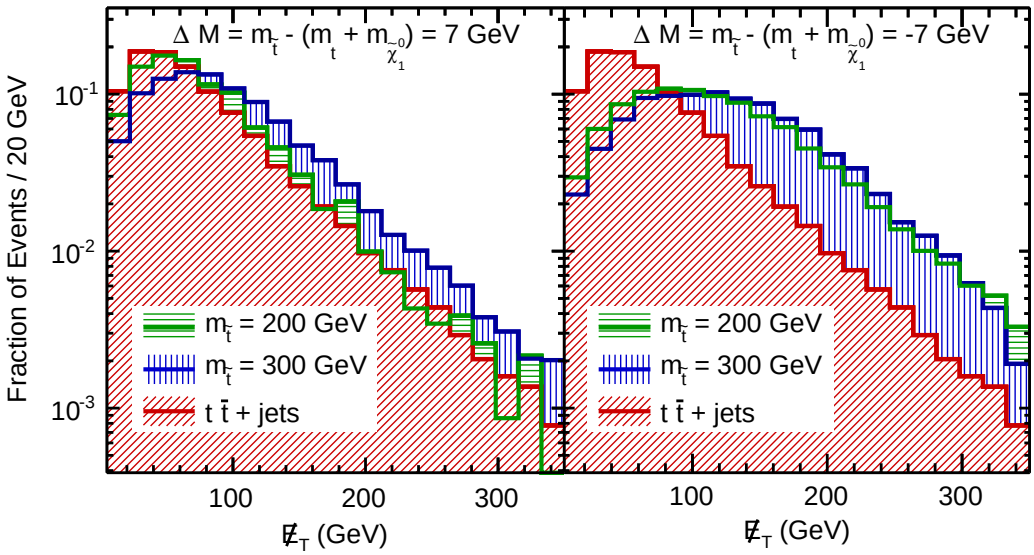

Figure 3.1: Distributions of $\not\!\!E_{\rm T}$ normalized to unity for signal (green horizontally dashed histogram) and $t\bar{t}$+jets background (red diagonally dashed histogram) after VBF selections and lepton and b-jet requirements for the benchmark point with $m_{\tilde{t}} = 400$ GeV, $m_{\tilde{\chi}^0_1} = 220$ GeV. Reprinted with permission from [1]

The systematic uncertainties are incorporated via nuisance parameters following the frequentist approach. A local p-value is calculated as the probability under a background only hypothesis to obtain a value of the test statistic as large as that obtained with a signal plus background hypothesis. The significance z is then determined as the value at which the integral of a Gaussian between z and ∞ results in a value equal to the local p-value. We find that the significance for $m_{\tilde{t}}$ = 200 GeV and $\Delta M = -7$ GeV is expected to be 4(2)σ for 300 fb^{-1} luminosity with 3(5)% systematic uncertainty, while the significance becomes 6(3)σ for $\Delta M = 7$ GeV.

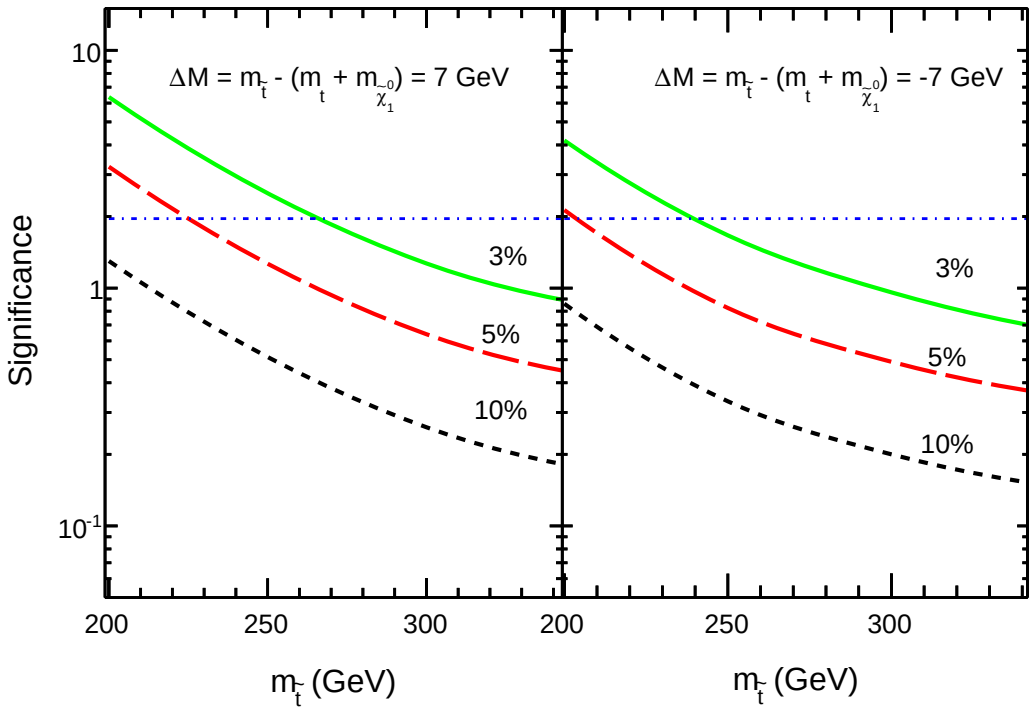

Figure 3.2: Significance as a function of $m_{\tilde{t}}$ for the $\Delta M = \pm 7$ GeV for 3, 5 and 10% systematics with integrated luminosities of 300 fb^{-1} at LHC14. The horizontal dotted line indicates 1.96 σ or 95% CL exclusion. Reprinted with permission from [1]

3.5 Discussion

The main result of this paper is that the VBF topology can provide a feasible strategy to search for compressed top squarks. A major improvement over non-VBF searches in the compressed scenario is the efficacy of the $\not{E}_{\rm T}$ cut, due to the fact that top squarks are indirectly produced (e.g. by weak bosons, gluons, squarks, etc.) with a pair of high $E_{\rm T}$ tagging jets. We note that in the stealthy scenario, the $\tilde{\chi}_1^0$ becomes massless, and the $\not{E}_{\rm T}$ cut loses its efficacy. We find that for ΔM =7 GeV $m_{\tilde{t}} \sim 390$ GeV (320 GeV) can be probed at 3σ (5σ) level with 300 fb^{-1} of integrated luminosity using $S/\sqrt{S+B}$. For the three body case with $\Delta M = -7$ GeV, the reach for $\tilde{t}$ is 320 (275) GeV at 3σ (5σ) with 300 fb^{-1}. The significance gets degraded when systematic uncertainties are taken into account. The significance for $m_{\tilde{t}}$ = 200 GeV and $\Delta M = 7$ GeV is expected to be 6(3)σ for 300 fb^{-1} luminosity with 3(5)% systematic uncertainty, while the significance becomes 4(2)σ for the same stop mass with $\Delta M = -7$ GeV. There are no constraints for this parameter space point from the present data nor the ATLAS and CMS projections for the upcoming run. We also note that the shape of the $\not{E}_{\rm T}$ distribution shows difference between $\Delta M = 7$ and $\Delta M = -7$ GeV. The determination of the systematic uncertainties due to the high pile-up conditions of the future is beyond the scope of this paper. It must be revisited with the expected performance of the upgraded ATLAS and CMS detectors.

4. HIGGS PORTAL DARK MATTER

4.1 Overview

Since the discovery of the Higgs boson in 2012, the ATLAS and CMS collaborations have placed strong constraints on potential models of physics beyond the standard model [26, 27, 28]. Measurements of couplings of the Higg's boson show strong agreement with standard model predictions [29]. These measurements provide constraints on contributions to the Higg's boson width from non standard model decays. This provides an upper limit on the branching ratio of Higgs to non-SM decays at .34 at 95% confidence level [29].

However, a number of models beyond the standard model allow for invisible decay modes of the Higgs boson within this limit. Such "Higgs Portal" models, allow the Higgs boson to act as a mediator between the standard model and dark matter particles. These Higgs Portal Dark Matter (HPDM) models can be probed at the LHC to test for dark matter. Of these HPDM models, Higgs portal fermion, scalar, and vector DM models are relatively simple. They are phenomenlogically interesting as the provide strong connections to the observed 125 GeV Higgs boson.

The following three sections establish the fermionic, scalar, and vector DM models. Then we consider two different decay mechanisms for HPDM. The first is vector boson fusion. In this case, we consider fermionic dark matter that couples to the Higgs. We apply cuts consistent with CMS's study [30], and provide the mass reach for 3 and 5 σ significance at 300, 1000, and 3000 fb^{-1} integrated luminosity. We also consider how VBF production of HPDM differs from similar production of Wino DM and how this difference is manifested in the distribution of $\not{E}_{\mathrm{T}}$

The second decay mechanism we consider is the associated production of Higgs and a Z boson. This scenario provides an interesting topology to study as the Z boson boosts

the Higgs boson in the transverse plane. We consider a comparision between kinematic distributions for fermionic, scalar, and vector DM after cuts in order to see if these three scenarios can be differentiated from one another as has been done for studys at the International Linear Collider (ILC). This consideration is made for both two leptons and 0 jets and two leptons and 1 jet. We also look more closely at how changing the width of the Higgs boson in the fermionic case can affect these distributions.

4.2 Higgs Portal Scalar DM Model

In the scalar case, the model is quite simple:

$$\mathcal{L}_{\text{scalarDM}} = \frac{1}{2}\partial_\mu S \partial^\mu S - \frac{1}{2}m_0^2 S^2 - \lambda_{HS} H^\dagger H S^2 - \frac{\lambda_S}{4!}S^4 \tag{4.1}$$

Using this Lagrangian, the $\not{E}_T$ distribution for the LHC can be calculate. The amplitude for $W^-(p_1)W^+(p_2) \to H \to S(k_1)S(k_2)$ is :

$$\mathcal{M}_{\text{scalar}} = \frac{2m_W^2}{v}\,\epsilon_W(p_1)\cdot\epsilon_W(p_2)\frac{1}{\hat{s} - m_H^2 + im_H\Gamma_H}\,2\lambda_{HS}v \tag{4.2}$$

$$= \mathcal{M}(W^-W^+ \to H)\frac{1}{\hat{s} - m_H^2 + im_H\Gamma_H}\,2\lambda_{HS}v \tag{4.3}$$

where $m_{12}^2 = (k_1 + k_2)^2 = m_{SS}^2 \equiv t$ is the invariant mass squared of the scalar DM pair, and $2\lambda_{HS}v$ is the DM coupling to the SM Higgs boson.

Here

$$\mathcal{M}(W^-W^+ \to H) = \frac{2m_W^2}{v}\,\epsilon_W(p_1)\cdot\epsilon_W(p_2),$$

is common to all three DM models in consideration.

Then the spin-averaged $\overline{|\mathcal{M}|^2} \equiv \sum_{spin}|\mathcal{M}|^2$ is given by

$$\overline{|\mathcal{M}|^2} = \frac{1}{3^2}\,\frac{1}{(\hat{s} - m_H^2)^2 + m_H^2\Gamma_H^2} \times (2v\lambda_{HS})^2\,\left[2 + \frac{(\hat{s} - 2m_W^2)^2}{4m_W^4}\right] \tag{4.4}$$

4.3 Higgs Portal Singlet Fermion DM Model

In the case of fermionic DM, we assume that the DM is a singlet Dirac fermion. We also assume it to have some dark charge in order to distinguish it from right-handed neutrinos.

$$\begin{aligned}\mathcal{L}_{\rm SFDM} = \overline{\chi}(i\partial\!\!\!/ - m_\chi - \lambda S)\chi + \frac{1}{2}\partial_\mu S \partial^\mu S - \frac{1}{2}m_0^2 S^2 \\ - \lambda_{HS} H^\dagger H S^2 - \mu_S S H^\dagger H - \mu_0^3 S - \frac{\mu_S}{3!}S^3 - \frac{\lambda_S}{4!}S^4.\end{aligned} \tag{4.5}$$

By expanding both fields about their vacuume expectation values($\langle H\rangle = v_H, \langle S\rangle = v_s$), the Lagrangian terms for h and s can derived. Diagonalization of the mass matrix, gives the DM χ coupling to both H_1 and H_2.

The interaction Lagrangian of H_1 and H_2 with the SM fields and DM χ is given by [31]:

$$\begin{aligned}\mathcal{L}_{\rm int} = -(H_1\cos\alpha + H_2\sin\alpha)\left[\sum_f \frac{m_f}{v_H}\overline{f}f - \frac{2m_W^2}{v_H}W_\mu^+ W^{-\mu} - \frac{m_Z^2}{v_H}Z_\mu Z^\mu\right] \\ + \lambda(H_1\sin\alpha - H_2\cos\alpha)\overline{\chi}\chi\ ,\end{aligned} \tag{4.6}$$

The 125 GeV scalar boson H_1 is the SM Higgs. The Higgs signal strength at the LHC is suppressed through the mixing of h and s independent of production and decay channels [31]. By using current data for the Higgs signal strength and the provided limit on Higgs to invisible branching ratio, the upper bound can be established. This bound is not however strigent and can be improved upon by future experiments.

The $\not{E}_T$ distribution at the LHC can be calculated using the following Lagrangian. In order to establish the amplitude for $W^-(p_1)W^+(p_2) \to H_{1,2} \to \chi\overline{\chi}$:

$$\mathcal{M}_{\rm SFDM} = \frac{2m_W^2}{v}\,\lambda\sin\alpha\cos\alpha\ \ \epsilon_W(p_1)\cdot\epsilon_W(p_2)$$

$$\times \left[\frac{1}{\hat{s}-m_1^2+im_1\Gamma_1}-\frac{1}{\hat{s}-m_2^2+im_2\Gamma_2}\right]\ \overline{u(k_1)}v(k_2) \tag{4.7}$$

$$= \mathcal{M}(W^-W^+\to H)\ \lambda \sin\alpha\cos\alpha$$

$$\times \left[\frac{1}{\hat{s}-m_1^2+im_1\Gamma_1}-\frac{1}{\hat{s}-m_2^2+im_2\Gamma_2}\right]\ \overline{u(k_1)}v(k_2) \tag{4.8}$$

$\mathcal{M}(W^-W^+\to H)$ was estbalished in the previous section. After summing over spins, fermionic DM aquires the following factor:

$$\sum |\overline{u(k_1)}v(k_2)|^2 = 4(k_1\cdot k_2 - m_\chi^2) = 2(\hat{s}-4m_\chi^2) \tag{4.9}$$

The amplitude squared vanishes near the threshold, where $\hat{s}\approx 4m_\chi^2$. This is due to the P-wave suppression of the cross sectio. This is different from the scalar and vector cases. It is our hope that because of this difference, there will be distguishing features between scalar, vector, and fermionic DM cases.

$$\overline{|\mathcal{M}|^2} = \frac{1}{3^2}\ \left|\frac{1}{\hat{s}-m_1^2+im_1\Gamma_1}-\frac{1}{\hat{s}-m_2^2+im_2\Gamma_2}\right|^2\ \left[2+\frac{(\hat{s}-2m_W^2)^2}{4m_W^4}\right]\ 2\left[\hat{s}-4m_\chi^2\right] \tag{4.10}$$

4.4 Higgs Portal Vector DM Model

While there are many different models for stable vector DM V_μ that couple to Higgs, here we will present a simplified case. In this case, we consider a discrete Z_2 symmetry ($V_\mu\to -V_\mu$) that is imposed by hand [32].

VEV provides a nonzero mass to vector DM V_μ. In order to satisfy theoretical constraints of renormalizability and unitarity, it is important to assume a gauge symmetry $U(1)_{dark}$ and dark Higgs Φ_X such that the vacuum expectation value provides a non-zero DM mass. More sophisticated models that include non-Abelian VDM from a gauged hid-

den sector can also be considered, but won't be discussed in this work [33, 34].

The Lagrangian for this simplified model is as follows:

$$\mathcal{L}_{\rm VDM} = -\frac{1}{4}V_{\mu\nu}V^{\mu\nu} + \frac{1}{2}m_V^2 V_\mu V^\mu(1+\frac{\phi}{v_\phi})^2 + \frac{1}{2}\partial_\mu\phi\partial^\mu\phi - \lambda_{\phi H}(vh+\frac{1}{2}h^2)(v_\phi\phi+\frac{1}{2}\phi^2) \tag{4.11}$$

After symmetry breaking we diagonalize the (h,ϕ) system Here $m_V = g_X v_\phi$.

For our purposes of studying $\not{E}_{\rm T}$ distributions at collider experiments, it suffices to truncate the model so as to neglect the cubic and quartic couplings of H_1 and H_2

$$\begin{aligned}\mathcal{L}_{\rm VDM} = &-\frac{1}{4}V_{\mu\nu}V^{\mu\nu} + \frac{1}{2}m_V^2 V_\mu V^\mu - \frac{m_V^2}{v_\phi}V_\mu V^\mu(H_1\sin\alpha - H_2\cos\alpha) \\ &- (H_1\cos\alpha + H_2\sin\alpha)\left[\sum_f \frac{m_f}{v_H}\bar{f}f - \frac{2m_W^2}{v_H}W_\mu^+ W^{-\mu} - \frac{m_Z^2}{v_H}Z_\mu Z^\mu\right]\end{aligned} \tag{4.12}$$

Using this Lagragian, it is possible to study the $\not{E}_{\rm T}$ distribution at the LHC. We begin by considering the amplitude for $W^-(p_1)W^+(p_2) \to H_{1,2} \to V(k_1)V(k_2)$:

$$\begin{aligned}\mathcal{M}_{\rm VDM} &= \frac{2m_W^2}{v}\,\frac{2m_V^2}{v_\phi}\,\epsilon_W(p_1)\cdot\epsilon_W(p_2) \\ &\times\left[\frac{1}{\hat{s}-m_1^2+im_1\Gamma_1} - \frac{1}{\hat{s}-m_2^2+im_2\Gamma_2}\right]\epsilon_V^*(k_1)\cdot\epsilon_V^*(k_2) \qquad (4.13)\\ &= \mathcal{M}(WW\to H)\frac{m_V^2}{v_\phi} \\ &\times\left[\frac{1}{\hat{s}-m_1^2+im_1\Gamma_1} - \frac{1}{\hat{s}-m_2^2+im_2\Gamma_2}\right]\epsilon_V^*(k_1)\cdot\epsilon_V^*(k_2) \qquad (4.14)\end{aligned}$$

Summing over VDM spins yields the following factor:

$$\sum|\epsilon_V^*(k_1)\cdot\epsilon_V^*(k_2)|^2 = 2 + \frac{(k_1\cdot k_2)^2}{m_V^4} = 2 + \frac{(\hat{s}-2m_V^2)^2}{4m_V^4} \tag{4.15}$$

The amplitude squared does not vanish near threshold, $\hat{s} \approx 4m_\chi^2$. This provides a distinc-

tive feature to differentiate this case from scalar and fermionic DM whcih can provide an observable at the LHC or ILC.

$$\overline{|\mathcal{M}|^2} = \frac{1}{3^2}\left|\frac{1}{\hat{s}-m_1^2+im_1\Gamma_1}-\frac{1}{\hat{s}-m_2^2+im_2\Gamma_2}\right|^2\left[2+\frac{(\hat{s}-2m_W^2)^2}{4m_W^4}\right]\left[2+\frac{(\hat{s}-2m_V^2)^2}{4m_V^4}\right] \tag{4.16}$$

4.5 VBF Production of HPDM

In this scenario, we consider the dijet + $\not{E}_T$ channels at LHC in order to probe the Higgs portal DM models where DM is fermionic. The parton level process follows:

$$q\bar{q}^{'} \rightarrow q\bar{q}^{'}W^-W^+,\;\; qq^{'} \rightarrow qq^{'}Z^0Z^0,\;\; q\overline{q^{'}} \rightarrow q\overline{q^{'}}Z^0Z^0 \tag{4.17}$$

followed by

$$W^-W^+, Z^0Z^0 \rightarrow H_{1,2} \rightarrow XX \tag{4.18}$$

where X indicates fermionic DM. Depending on the mass spectra and the initial parton CM energy $\sqrt{\hat{s}}$, H_1 or H_2 can either be on-shell or off-shell. Here we consider off-shell production. Figure 4.1 shows the Feynman diagram associated with this production.

4.5.1 Search Strategy

In order to study the VBF production of HPDM, we consider three benchmark points for DM mass(Higgs mass): 50(200), 100(300), and 200(500) GeV. For the on-shell case, we use a branching ratio from SM Higgs to DM of 20%. In the 100 and 200 GeV cases, we use branching ratios of h_2 30% and 15% respectively.

We simulate these benchmark points by using `MADGRAPH5`. Parton showering is handled by `PYTHIA`. The detector simulation is provided by `DELPHES`

To select the VBF topology, we follow the cutflow provided by CMS [30]:

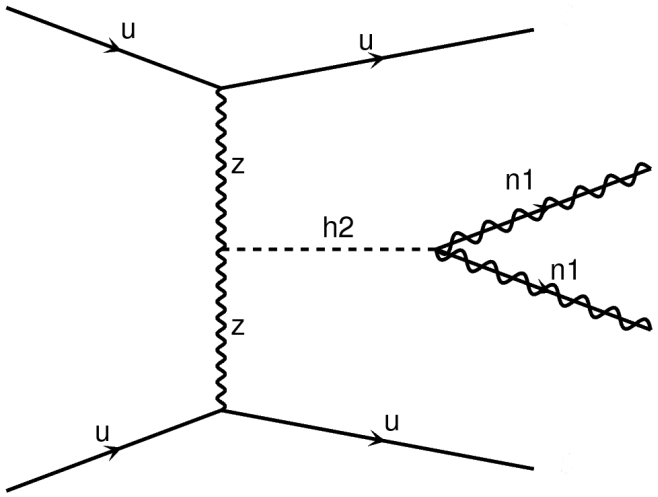

Figure 4.1: Feynman Diagram for VBF production of fermionic DM through Higgs.

- At least 2 Jets p_T > 30
- No leptons p_T > 10 GeV
- Leading Jet p_T > 80 GeV
- Subleading Jet p_T > 70 GeV
- m_{jj} > 1100 GeV
- min($\Delta\phi(j, \not{E}_{\mathrm{T}})$)>2.3
- $\Delta(\eta_1, \eta_2) > 3.5$ & $\eta_1 \cdot \eta_2 < -1$

The dominant sources of background are $Z(\nu\nu) + jets$ and $W(l\nu) + jets$. We use the background estimations provided by CMS [30].

4.5.2 Results

The results for our three benchmark points are summarized in 4.1. From the CMS analysis, the cross section of inclusive background is 54.3 fb. By using this background

estimation and our cutflow for our benchmark points, we calculate and plot the significance $S/\sqrt{S+B}$ in Figure 4.2. We see 3(5)σ signficance for DM mass of 170(195) GeV.

We are also interested in showing the difference in the distribution of $\not{E}_{\mathrm{T}}$ after the cuts in Table 4.1 to see how this compares to the case of wino DM. We plot the distribution of $\not{E}_{\mathrm{T}}$ for these two scenarios in Figure 4.3. The difference in these cases can be understood by considering the VBF processes for the two models. In the HPDM case, DM is produced by an s-channel Higgs as seen in Figure 4.1. In the wino case, DM is produced by a t-channel process as seen in Figure 4.4.

4.6 Z + H Production of HPDM

Here we consider Z + $\not{E}_T$ where $\not{E}_T$ is from the Higgs couplings to the DM pair:

$$q\overline{q'} \to Z^* \to ZH_{1,2} \to ZXX.$$

Here intermediate $H_{1,2}$ could be either on-shell or off-shell. X denotes DM. We consider leptonic decays of Z.

4.6.1 Search Strategy

In order to search for these decays, we generate samples that have final states with a Z boson and a Higgs for the cases of fermionic, scalar, and vector DM. In the fermionic and vector case the Higgs has a mass of 300 GeV and the DM has a mass of 100 GeV. The scarlar case has a DM mass of 100 GeV. We expect decays of this type to have a topology in which the Higgs will recoil against the Z boson or the initial state radiation. As such, we apply cuts to select on this boosted system [30]. We then consider leptonic decays with 0 and 1 additional jet. In all cases, we require the particles coming from the Z boson to have an invariant mass within 15 GeV of the Z boson mass and a $\not{E}_{\mathrm{T}}$ cut of at least 100 GeV. We follow the cutflow prescribed by CMS [30].

Table 4.1: Cutflow for 50, 100, and 200 GeV DM benchmark points for VBF production of fermionic HPDM. Summary of the effective cross-sections in (fb). Masses and momenta are in GeV.

(m_{DM}, m_{h_2})	Cuts	Cross Section (fb)
$(50, 200)$	Pre cut	427
	At least 2 Jets p_T > 30 GeV	284
	No leptons p_T > 10 GeV	284
	Leading Jet p_T > 80 GeV	163
	Subleading Jet p_T > 70 GeV	63
	m_{jj} > 1100 GeV	13
	$\not{E}_{\mathrm{T}} > 200$	3.7
	min($\Delta\phi(j, \not{E}_{\mathrm{T}})$)>2.3	2.1
	$\Delta(\eta_1, \eta_2) > 3.5$ & $\eta_1 \cdot \eta_2 < -1$	2.1
$(100, 300)$	Pre cut	195
	At least 2 Jets p_T > 30 GeV	138
	No leptons p_T > 10 GeV	138
	Leading Jet p_T > 80 GeV	90
	Subleading Jet p_T > 70 GeV	37
	m_{jj} > 1100 GeV	12
	$\not{E}_{\mathrm{T}} > 200$	4
	min($\Delta\phi(j, \not{E}_{\mathrm{T}})$)>2.3	2.3
	$\Delta(\eta_1, \eta_2) > 3.5$ & $\eta_1 \cdot \eta_2 < -1$	2.3
$(200, 500)$	Pre cut	23
	At least 2 Jets p_T > 30 GeV	16
	No leptons p_T > 10 GeV	16
	Leading Jet p_T > 80 GeV	10
	Subleading Jet p_T > 70 GeV	4.7
	m_{jj} > 1100 GeV	1.8
	$\not{E}_{\mathrm{T}} > 200$	.70
	min($\Delta\phi(j, \not{E}_{\mathrm{T}})$)>2.3	.40
	$\Delta(\eta_1, \eta_2) > 3.5$ & $\eta_1 \cdot \eta_2 < -1$	.39

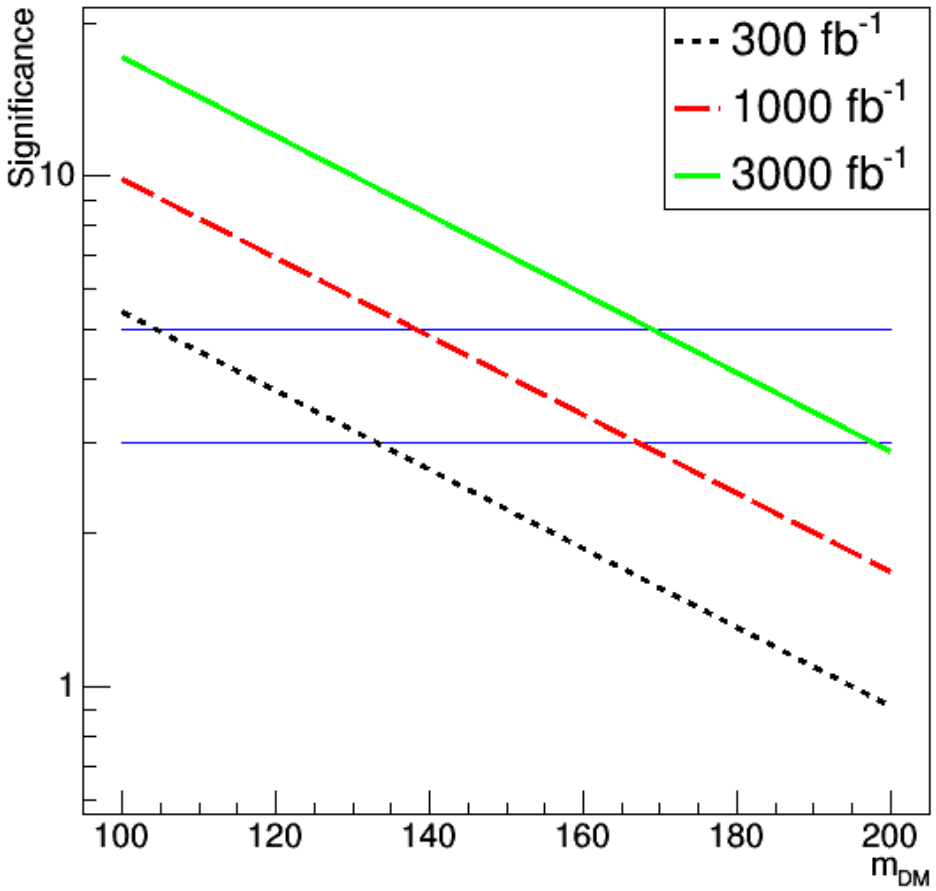

Figure 4.2: Significance vs. Mass for fermionic HPDM for the VBF secnario after cuts in Table 4.1. Significance is calculated as $\frac{S}{\sqrt{S+B}}$

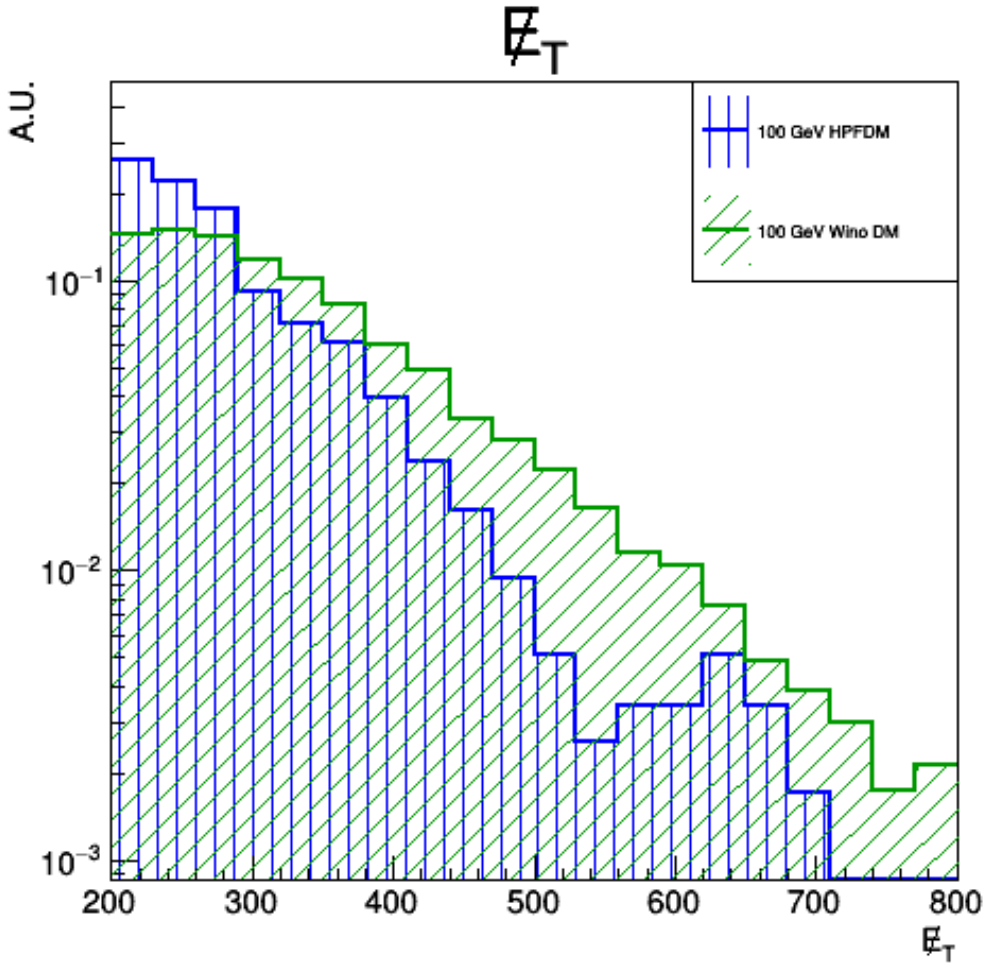

Figure 4.3: Shape comparison between $\not{E}_{\mathrm{T}}$ for VBF production of fermionic HPDM and Wino Dark matter. After all cuts in Table 4.1

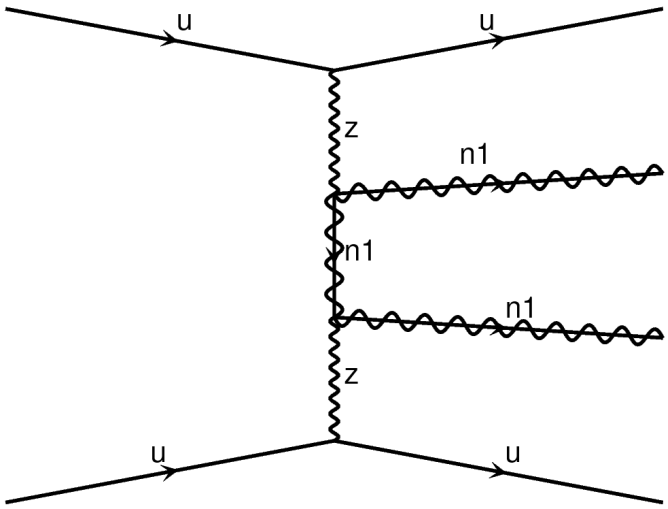

Figure 4.4: Feynman Diagram for VBF production of Wino dark matter

4.6.2 Results

Tables 4.2, 4.2, and 4.2 summarize the cross sections for the three scenarios cut by cut. We see similarity in cross section for the fermionic and vector cases as DM decays from the on-shell h_2. The cross section is suppressed in the scalar case due to the fact that Higgs decay is off-shell. Figures 4.5 and 4.6 show the distributions of m_T, $\not{E}_{\mathrm{T}}$, $\Delta\phi(l_1, l_2)$, and p_T^{ll}. Here m_T is defined as the transverse mass between the $\not{E}_{\mathrm{T}}$ and the dilepton system. We see some discrimination between the scalar and the vector and fermionic cases. The fact that the scalar DM decay is offshell is the primary reason for the difference in the distributions in Figure 4.5. A χ squared analysis could qualify this discrimination. We see no discrimination between the fermionic and vector cases.

In figures 4.7 and 4.8, we explore if there is a distinction between h_2 for the fermionic case with a 12 GeV width and 48 GeV width for the 0 and 1 jet case respectively. We see very little distinction between these two cases.

Table 4.2: Cutflow for 100 GeV DM benchpark point for HZ production of fermionic HPDM in 0 and 1 jet channels. Summary of the effective cross-sections in (fb). Masses and momenta are in GeV.

(m_{DM}, m_{h_2})	Cuts	Cross Section (fb)
$(100, 300)$	Pre cut	8.4
0 Jets	No Jets p_T > 30 GeV	1.3
	2 OSSF Leptons p_T > 20 GeV	.15
	$\lvert m_{ll} - m_Z \rvert$ < 15 GeV	.15
	$\Delta\phi(l_1, l_2) < \frac{\pi}{2}$ GeV	.11
	$\not{E}_{\mathrm{T}} > 100GeV$	.098
	$\Delta\phi(ll, \not{E}_{\mathrm{T}}) > 2.8$	.097
	$\frac{\lvert \not{E}_{\mathrm{T}} - p_T^{ll} \rvert}{p_T^{ll}} < .4$	.097
	$m_T > 200$	.097
$(100, 300)$	Pre cut	.84
1 Jet	Exactly 1 Jet p_T > 30 GeV	2.2
	2 OSSF Leptons p_T > 20 GeV	.072
	$\lvert m_{ll} - m_Z \rvert$ < 15 GeV	.071
	$\Delta\phi(l_1, l_2) < \frac{\pi}{2}$ GeV	.054
	$\not{E}_{\mathrm{T}} > 100GeV$	.048
	$\Delta\phi(ll, \not{E}_{\mathrm{T}}) > 2.8$	.035
	$\Delta\phi(j, \not{E}_{\mathrm{T}}) > .5$	.030
	$\frac{\lvert \not{E}_{\mathrm{T}} - p_T^{ll} \rvert}{p_T^{ll}} < .4$	.028
	$m_T > 200$	.028

Table 4.3: Cutflow for 100 GeV DM benchpark point for HZ production of scalar HPDM in 0 and 1 jet channels. Summary of the effective cross-sections in (fb). Masses and momenta are in GeV.

(m_{DM})	Cuts	Cross Section (fb)
(100)	Pre cut	.81
0 Jets	No Jets p_T > 30 GeV	.13
	2 OSSF Leptons p_T > 20 GeV	.015
	$\lvert m_{ll} - m_Z \rvert$ < 15 GeV	.014
	$\Delta\phi(l_1, l_2) < \frac{\pi}{2}$ GeV	9.4×10^{-3}
	$\not{E}_{\mathrm{T}} > 100GeV$	8.2×10^{-3}
	$\Delta\phi(ll, \not{E}_{\mathrm{T}}) > 2.8$	8.2×10^{-3}
	$\frac{\lvert \not{E}_{\mathrm{T}} - p_T^{ll} \rvert}{p_T^{ll}} \rvert < .4$	8.1×10^{-3}
	$m_T > 200$	8.1×10^{-3}
(100)	Pre cut	.81
1 Jets	Exactly 1 Jet p_T > 30 GeV	.23
	2 OSSF Leptons p_T > 20 GeV	6.5×10^{-3}
	$\lvert m_{ll} - m_Z \rvert$ < 15 GeV	6.5×10^{-3}
	$\Delta\phi(l_1, l_2) < \frac{\pi}{2}$ GeV	4.4×10^{-3}
	$\not{E}_{\mathrm{T}} > 100GeV$	3.6×10^{-3}
	$\Delta\phi(ll, \not{E}_{\mathrm{T}}) > 2.8$	2.6×10^{-3}
	$\Delta\phi(j, \not{E}_{\mathrm{T}}) > .5$	2.2×10^{-3}
	$\frac{\lvert \not{E}_{\mathrm{T}} - p_T^{ll} \rvert}{p_T^{ll}} \rvert < .4$	2.0×10^{-3}
	$m_T > 200$	2.0×10^{-3}

Table 4.4: Cutflow for 100 GeV DM benchpark point for HZ production of vector HPDM in 0 and 1 jet channels. Summary of the effective cross-sections in (fb). Masses and momenta are in GeV.

(m_{DM})	Cuts	Cross Section (fb)
$(100, 300)$	Pre cut	8.4
0 Jets	No Jets p_T > 30 GeV	1.3
	2 OSSF Leptons p_T > 20 GeV	.15
	$\|m_{ll} - m_Z\|$ < 15 GeV	.15
	$\Delta\phi(l_1, l_2) < \frac{\pi}{2}$ GeV	.11
	$\not{E}_{\mathrm{T}} > 100GeV$	.099
	$\Delta\phi(ll, \not{E}_{\mathrm{T}}) > 2.8$	.099
	$\frac{\|\not{E}_{\mathrm{T}} - p_T^{ll}\|}{p_T^{ll}}\| < .4$	.099
	$m_T > 200$	.099
$(100, 300)$	Pre cut	.84
0 Jets	No Jets p_T > 30 GeV	2.3
	2 OSSF Leptons p_T > 20 GeV	.071
	$\|m_{ll} - m_Z\|$ < 15 GeV	.070
	$\Delta\phi(l_1, l_2) < \frac{\pi}{2}$ GeV	.054
	$\not{E}_{\mathrm{T}} > 100GeV$	.047
	$\Delta\phi(ll, \not{E}_{\mathrm{T}}) > 2.8$	.034
	$\Delta\phi(j, \not{E}_{\mathrm{T}}) > .5$	.029
	$\frac{\|\not{E}_{\mathrm{T}} - p_T^{ll}\|}{p_T^{ll}} < .4$	.026
	$m_T > 200$	.026

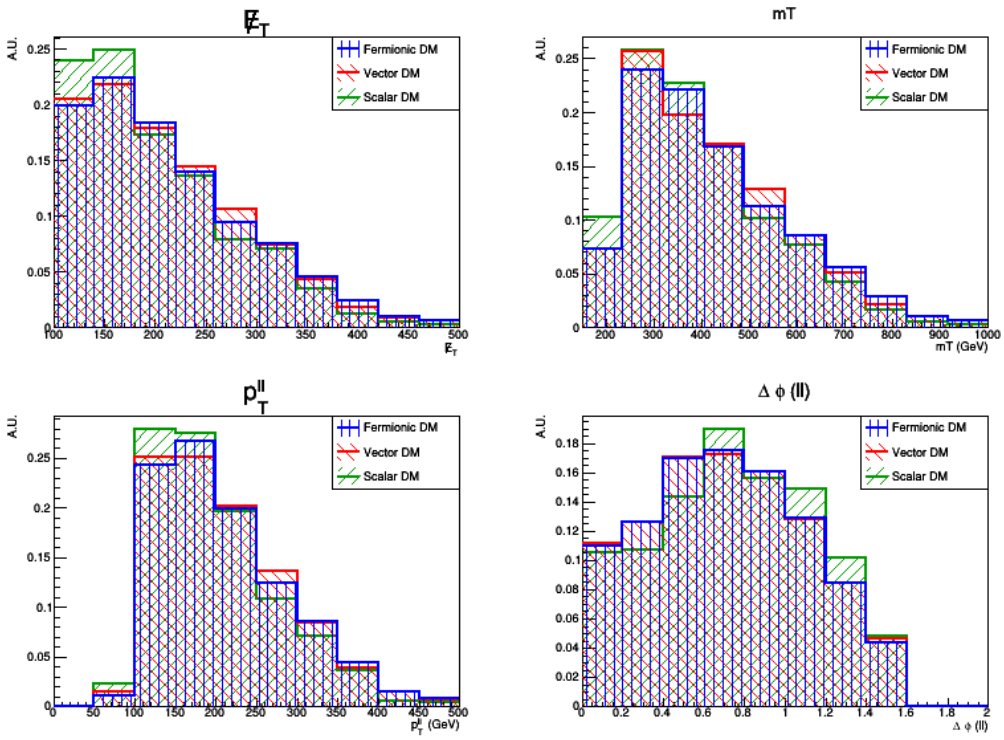

Figure 4.5: Comparison of kinematic distributions with 0 jets for fermionic, scalar, and vector dark matter in the boosted $H + Z$ scenario. After all cuts in Tables 4.2, 4.3, and 4.4.

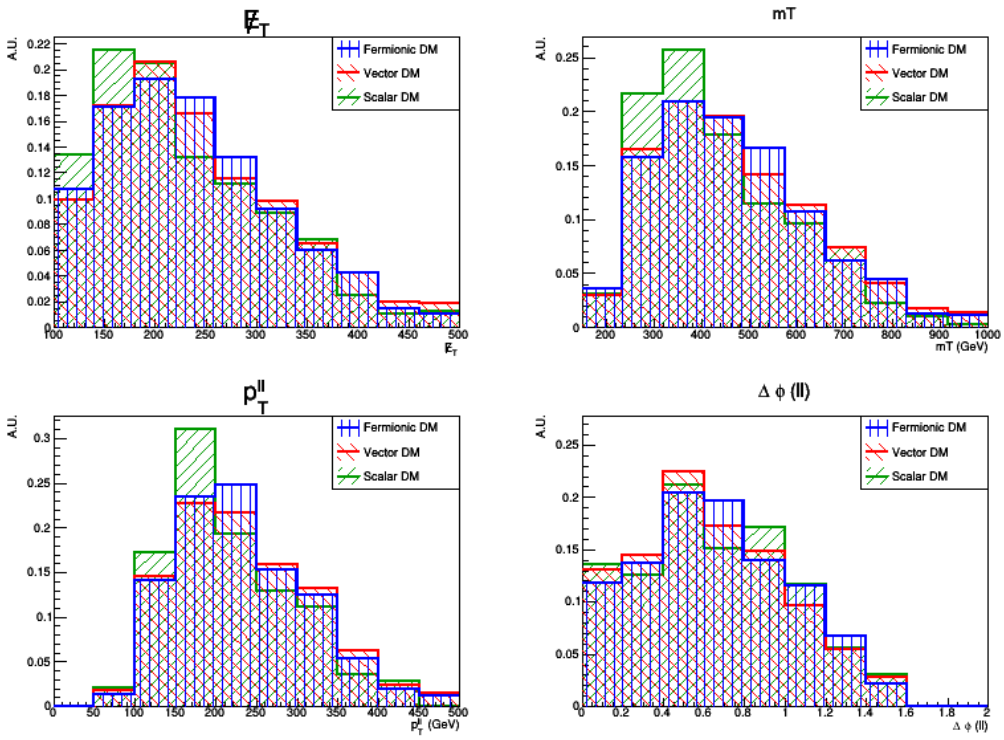

Figure 4.6: Comparison of kinematic distributions with 1 jet for fermionic, scalar, and vector dark matter in the boosted $H + Z$ scenario. After all cuts in Tables 4.2, 4.3, and 4.4.

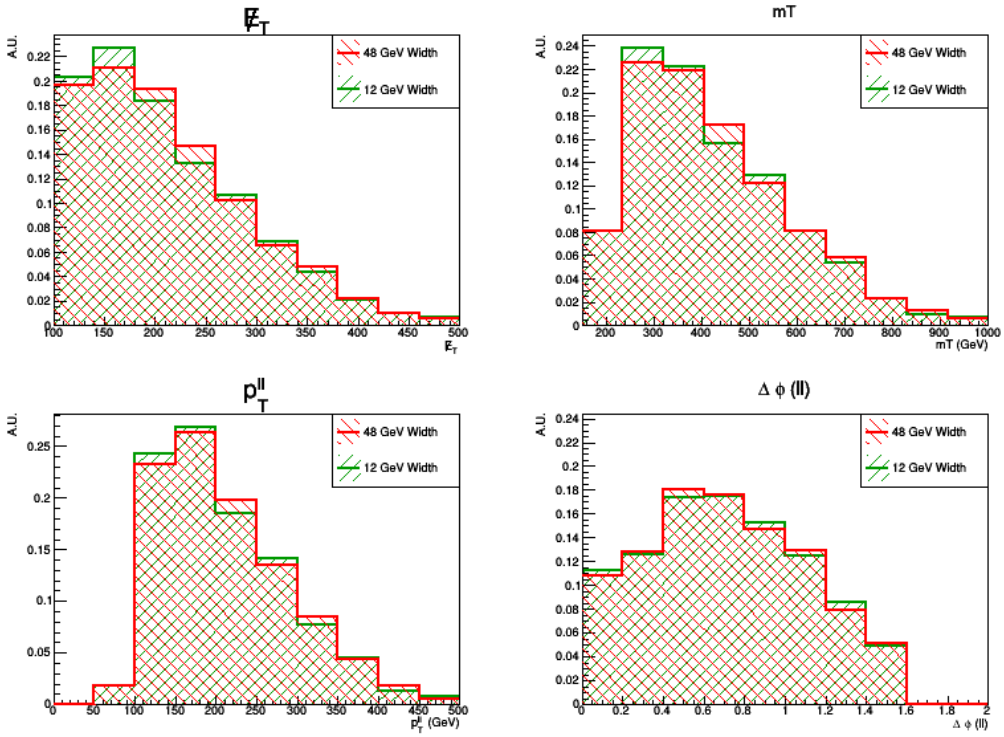

Figure 4.7: Comparison of kinematic distributions with 0 jets for fermionic dark matter with widths of 12 GeV and 48 GeV in the boosted $H + Z$ scenario. After all cuts in Tables 4.2, 4.3, and 4.4.

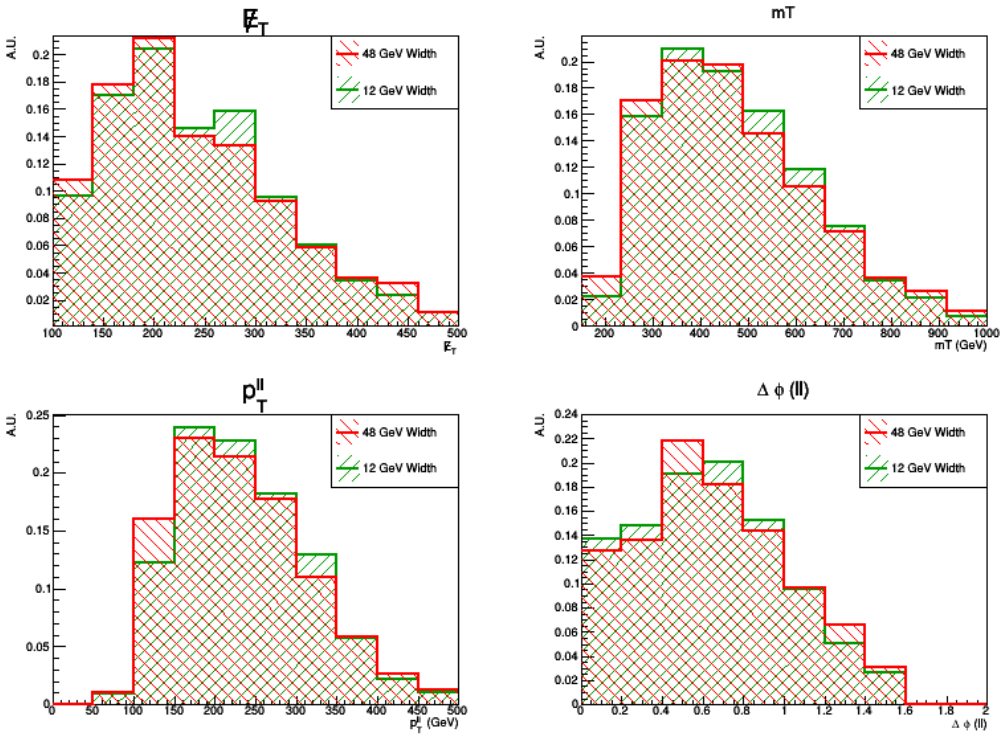

Figure 4.8: Comparison of kinematic distributions with 1 jet for fermionic dark matter with withs of 12 GeV and 48 GeV. After all cuts.

5. CONCLUSION

The standard model of particle physics has enjoyed a great deal of success. It successfully explains the interactions between quarks and leptons. With the discovery of the Higg's boson in 2012, it also explains how these particles gain their masses. The standard model is however not without its issues. It does not address the heirarchy problem, nor does it provide a particle explanation of dark matter. In order to address these issues, additional models must be consider. This work considered two models that address the dark matter content of the universe.

The first scenario we considered was the production of compressed $\tilde{t}$ quarks. This scenario is advantageous to study as coannihilation of compressed $\tilde{t}$ quarks in the early universe can recover the observed dark matter relic density. We showed that by using VBF topologies, $\not{E}_{\mathrm{T}}$ in the $\tilde{t}$ system can be enhanced. As a result, we can probe compressed $\tilde{t}$'s with a mass of 300 GeV at the 5 σ level with 300 fb^{-1} of integrated luminosity at the 14 TeV LHC.

The second senario we considered was an extension of Higgs sector physics. We considered VBF and $H + Z$ production of HPDM. In the VBF scenario, we showed that DM with a mass of 195 GeV can achieve 5 σ signficance at 3000 fb^{-1} in the case of fermionic DM. We also showed the differences in the distribution of $\not{E}_{\mathrm{T}}$ between fermionic HPDM and wino DM. In the case of $H + Z$ production of HPDM, we showed the kinematic distributions for fermionic, scalar, and vector DM after cuts. We did not see any difference between the vector and the fermionic case, but there was some discrimination between these two cases and the scalar case. We also showed that changing the width of fermionic DM does not result in appreciable changes in the kinematic distributions. We will be publishing these results later this summer.

REFERENCES

[1] B. Dutta, W. Flanagan, A. Gurrola, W. Johns, T. Kamon, P. Sheldon, K. Sinha, K. Wang, S. Wu, Phys. Rev. D **90**, 095022 (2014).

[2] G. Jungman, M. Kamionkowski and K. Griest, Phys. Rep. **267** (1996) 195.

[3] M. A. Ajaib, T. Li and Q. Shafi, Phys. Rev. D **85**, 055021 (2012) [arXiv:1111.4467 [hep-ph]].

[4] B. Dutta, T. Ghosh, A. Gurrola, W. Johns, T. Kamon, P. Sheldon, K. Sinha, K. Wang, S. Wu Phys. Rev. D **91**, 055025 (2015).

[5] ATLAS Collaboration, Phys. Rev. D **87**, 012008 (2013) [arXiv:1208.0949 [hep-ex]].

[6] ATLAS Collaboration, J. High Energy Phys. **07**, 167 (2012) [arXiv:1206.1760 [hep-ex]].

[7] CMS Collaboration, Phys. Rev. Lett. **109**, 171803 (2012) [arXiv:1207.1898 [hep-ex]].

[8] ATLAS Collaboration, ATLAS-CONF-2013-047.

[9] ATLAS Collaboration, ATLAS-CONF-2012-166.

[10] ATLAS Collaboration, ATLAS-CONF-2012-167.

[11] B. Dutta, T. Kamon, N. Kolev, K. Sinha and K. Wang, Phys. Rev. D **86**, 075004 (2012) [arXiv:1207.1873 [hep-ph]]. D. E. Kaplan, K. Rehermann and D. Stolarski, J. High Energy Phys. **07**, 119 (2012) [arXiv:1205.5816 [hep-ph]].

[12] T. Han, R. Mahbubani, D. G. E. Walker and L. -T. Wang, J. High Energy Phys. **05**, 117 (2009) [arXiv:0803.3820 [hep-ph]]. Y. Bai, H. -C. Cheng, J. Gallicchio and J. Gu, J. High Energy Phys. **07**, 110 (2012) [arXiv:1203.4813 [hep-ph]].

[13] M. R. Buckley, T. Plehn and M. Takeuchi, J. High Energy Phys. **08**, 086 (2013)[arXiv:1302.6238 [hep-ph]]. T. Plehn, M. Spannowsky and M. Takeuchi, J. High Energy Phys. **08**, 091 (2012) [arXiv:1205.2696 [hep-ph]].

[14] ATLAS White paper: ATL-PHYS-PUB-2013-007, http://arxiv.org/abs/1307.7292.

[15] CMS White paper: CMS NOTE-13-002, http://arxiv.org/abs/1307.7135.

[16] B. Dutta, T. Kamon, N. Kolev, K. Sinha, K. Wang and S. Wu, Phys. Rev. D **87**, 095007 (2013) M. L. Graesser and J. Shelton, Phys. Rev. Lett. **111**, 121802 (2013).

[17] D. S. M. Alves, M. R. Buckley, P. J. Fox, J. D. Lykken and C. -T. Yu, Phys. Rev. D **87**, no. 3, 035016 (2013).

[18] Z. Han, A. Katz, D. Krohn and M. Reece, J. High Energy Phys. **08**, 083 (2012) [arXiv:1205.5808 [hep-ph]].

[19] C. Kilic and B. Tweedie, J. High Energy Phys. **04**, 110 (2013) [arXiv:1211.6106 [hep-ph]].

[20] B. Dutta, A. Gurrola, W. Johns, T. Kamon, P. Sheldon and K. Sinha, Phys. Rev. D **87**, 035029 (2013).

[21] G. -C. Cho, K. Hagiwara, J. Kanzaki, T. Plehn, D. Rainwater and T. Stelzer, Phys. Rev. D **73**, 054002 (2006); A. Datta, P. Konar and B. Mukhopadhyaya, Phys. Rev. D **65**, 055008 (2002); Phys. Rev. Lett. **88**, 181802 (2002);.

[22] A. G. Delannoy, B. Dutta, A. Gurrola, W. Johns, T. Kamon, E. Luiggi, A. Melo and P. Sheldon *et al.*, Phys. Rev. Lett. **111**, 061801 (2013).

[23] J. Alwall, M. Herquet, F. Maltoni, O. Mattelaer and T. Stelzer, J. High Energy Phys. **06**, 128 (2011) [arXiv:1106.0522 [hep-ph]].

[24] T. Sjostrand, S. Mrenna and P. Z. Skands, J. High Energy Phys. **05**, 026 (2006) [hep-ph/0603175].

[25] PGS4 is a parameterized detector simulator. We use version 4 in the LHC detector configuration.

[26] ATLAS Collaboration, Phys. Lett. B **716** (2012) 1 arXiv:1207.7214 [hep-ph]].

[27] CMS Collaboration, Phys. Lett. B **716** (2012) 30 arXiv:1207.7235 [hep-ph]].

[28] CMS Collaboration, PHys. Lett. B **716** (2012) 081 arXiv:1303.4671 [hep-ph]].

[29] ATLAS,CMS Collaboration arXiv:1606.02266 [hep-ph]].

[30] "Searches for invisible Higgs boson decays with the CMS detector.," Tech. Rep. CMS-PAS-HIG-16-016, CERN, Geneva, 2016.

[31] S. Baek, P. Ko and W. I. Park, JHEP **1202**, 047 (2012) [arXiv:1112.1847 [hep-ph]].

[32] S. Baek, P. Ko, W. I. Park and E. Senaha, JHEP **1305**, 036 (2013) [arXiv:1212.2131 [hep-ph]].

[33] T. Hambye, JHEP **0901**, 028 (2009) [arXiv:0811.0172 [hep-ph]].

[34] S. Baek, P. Ko and W. I. Park, JCAP **1410**, no. 10, 067 (2014) [arXiv:1311.1035 [hep-ph]].